DOI: 10.1002/anie.201104829

VIP Purifying Heterodimers

Purification and Magnetic Interrogation of Hybrid Au-Fe_3O_4 and FePt-Fe_3O_4 Nanoparticles**

Jacob S. Beveridge, Matthew R. Buck, James F. Bondi, Rajiv Misra, Peter Schiffer, Raymond E. Schaak, and Mary Elizabeth Williams**

Hybrid heterodimer, -trimer, and -oligomer nanoparticles, which contain two or more domains connected through a solid-state interface, are of interest for catalysis, medicine, biodiagnostics, and electronics.[1] For example, the spatially distinct surfaces in M-Fe_3O_4 (M = Au, Pt, Pd) heterodimer nanoparticles[2–4] have been chemically derivatized with complementary ligands and used as target-specific drug-delivery vehicles[5] and dual-imaging biological probes.[6] Synergistic effects such as electron transfer and spin exchange can be mediated by nanoscale heterojunctions in hybrid nanocrystals, giving rise to properties that have been exploited in advanced catalysts,[2,7,8] exchange-coupled magnets,[9] magneto-optics,[10] electronics[11] and solar conversion devices.[12]

To synthesize hybrid nanoparticles, judicious selection of reaction conditions is needed to promote heterogeneous nucleation of a target solid onto preformed nanocrystal seeds while avoiding conditions that result in isolated single-component particles.[13,14] Despite the growing number of two-component heterodimers,[1b,15] pure samples in high yield are difficult to obtain, and heterogeneous seeded growth is challenging to control. For example, in the prototypical Au-Fe_3O_4 system, the seed size, seed crystallinity,[16] lattice matching,[2a] solvent polarity,[14] heating rate,[16] and stabilizer concentration all influence the final product morphology. The low purity of common commercially available stabilizers superimposes additional technical challenges with respect to reproducibility. Indeed, hybrid nanoparticle heterostructures and their syntheses are becoming increasingly complex and have the potential to form multiple products in the reaction solution.

[*] J. S. Beveridge, M. R. Buck, J. F. Bondi, Prof. R. E. Schaak, Prof. M. E. Williams
Department of Chemistry, The Pennsylvania State University
University Park, PA 16802 (USA)
E-mail: schaak@chem.psu.edu
mbw@chem.psu.edu
Dr. R. Misra, Prof. P. Schiffer
Department of Physics and Materials Research Institute
The Pennsylvania State University (USA)

[**] Funding for this project was provided by the National Science Foundation (to M.E.W. Grant CHE-0848701; to R.E.S. Grant CHE-0845258; and to P.S. the Penn State MRSEC DMR-0820404). We thank the Penn State Huck Institutes of the Life Sciences and Materials Research Institute electron microscopy facilities for their assistance.

Supporting information for this article is available on the WWW under http://dx.doi.org/10.1002/anie.201104829.

The macroscale-measured properties represent the ensemble averages of the constituent particle populations, so purification is critical for understanding the intrinsic structure–function relationships in these materials. Distinctly absent from the nanoparticle synthesis literature are post-synthetic separation and purification methods, and indeed there is a dearth of available methodologies for use with colloidal nanomaterials. However, while some nanoparticle purification methodologies exist,[17,18] quantitative separation and purification of colloidal nanoparticles is rarely practiced and has not previously been applied to hybrid nanoparticle systems. Accordingly, we describe here the purification and subsequent magnetic interrogation of hybrid magnetic nanoparticles using differential magnetic catch and release (DMCR), which is our recently reported chromatographic technique that separates polydisperse magnetic nanoparticles into monodisperse fractions based upon differences in their magnetic moments.[19] We use DMCR to generate purified fractions of the important hybrid nanocrystal systems Au-Fe_3O_4[14,16,20] and FePt-Fe_3O_4.[9] Interestingly, we observe substantially different magnetic properties in the purified heterostructures compared to the as-synthesized materials: different (more accurate) saturation magnetization values and the identification of magnetic polydispersity in morphologically similar hybrid nanoparticles that would not be detectable using established methods.

Details of the DMCR separation technique are provided in the Supporting Information and in Ref. [19]. Briefly, particles are separated using an open tubular fused silica capillary wrapped between two narrowly spaced electromagnet poles. The solvent mobile phase imparts a drag force (F_D) on the nanoparticles and a magnetic flux gradient, applied orthogonal to the direction of solvent flow, exerts a magnetic force (F_M) on the particles and pulls them against the capillary wall (Figure S1 in the Supporting Information). For any location in the capillary with equal flow rate, particles of identical composition, size, shape, and crystallinity have the same F_M and F_D acting on them. Variations in F_M and F_D in polydisperse samples are leveraged to separate particles in the DMCR apparatus.

Hybrid Au-Fe_3O_4 nanoparticles were synthesized by thermal decomposition of [$Fe(CO)_5$] in the presence of Au nanoparticle seeds.[2,3] Figure 1 shows the DMCR chromatogram in the absence of a magnetic field for a representative sample of as-synthesized colloidal Au-Fe_3O_4 nanoparticles; a single peak (A) elutes at the dead time of the column. Applying a magnetic field program (dashed line) results in a chromatogram with three peaks (B, C, D). The first of these (B) elutes while a 2 T magnetic flux density is applied,

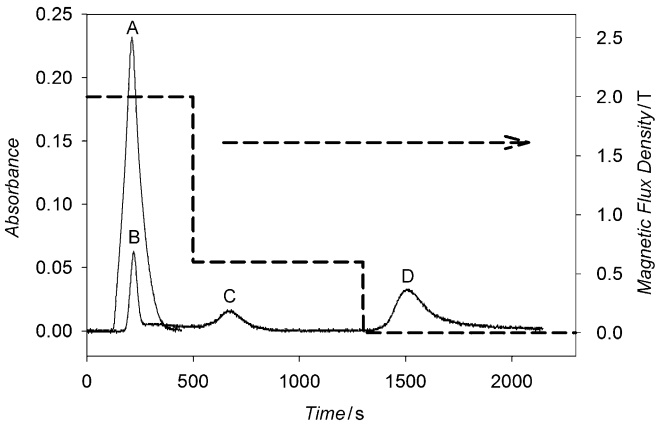

Figure 1. Peak A: elution of Au-Fe_3O_4 hybrid nanoparticles with no applied magnetic field. Peaks B, C, and D: DMCR chromatogram of the separation of the Au-Fe_3O_4 nanoparticles under the applied magnetic flux density indicated by the dashed line.

whereas peaks C and D elute when the field is dropped to 0.6 and 0 T, respectively. Because the order of elution of the peaks depends on the relationship between F_M and F_D for each particle, it is determined by either changes in effective size or magnetic moment.

Each fraction was collected as it eluted from the capillary, and representative transmission electron microscope (TEM) images for each fraction and for the initial sample are shown in Figure 2. Although some TEM images of the as-synthesized sample contained regions with predominantly hybrid particles (Figure 2a), comprehensive TEM examination revealed that 60% of the particles ($n = 94$; n: number of particles) consisted of individual nonhybrid particle impurities mixed with the intended hybrid nanoparticles. The particles eluting in peaks B and C are single, spherical particles with diameters of (7.0 ± 1.6) nm ($n = 308$) and (11.0 ± 1.3) nm ($n = 495$), respectively (Figure 2b,c). The TEM image of the particles eluted in peak D (Figure 2d) reveals hybrid nanostructures. The purified sample (peak D) contains 97% heterostructures ($n = 135$). With a constant mobile-phase velocity, the increase in cross-sectional area of the particles would result in an increased F_D (i.e., B < C < D). Therefore, the observed order of elution indicates a difference in magnetic moment, and reflects a larger total volume of Fe_3O_4 within the hybrid nanostructure versus within individual nanoparticles.

Selected area electron diffraction (SAED) patterns (Figure 2) confirm that both Au and Fe_3O_4 elute in peak A. While the ED patterns for particles from peaks B and C show only Fe_3O_4, the hybrid particles from peak D show evidence of both Au and Fe_3O_4. Energy dispersive X-ray spectra (EDS) (Figure S2) further confirm that the particles in peaks B and C contain only Fe, whereas those eluting in peak D contain both Au and Fe. Larger sample quantities were obtained by performing preparatory-scale DMCR,[19b] which incrementally purifies the sample in about 2 mg injections while retaining the fidelity of the separation (Figure S3). UV/vis absorption spectra obtained for each fraction also confirm the presence of Au in peaks A and D but not in B and C (Figure S4). Taken together, the data provide important

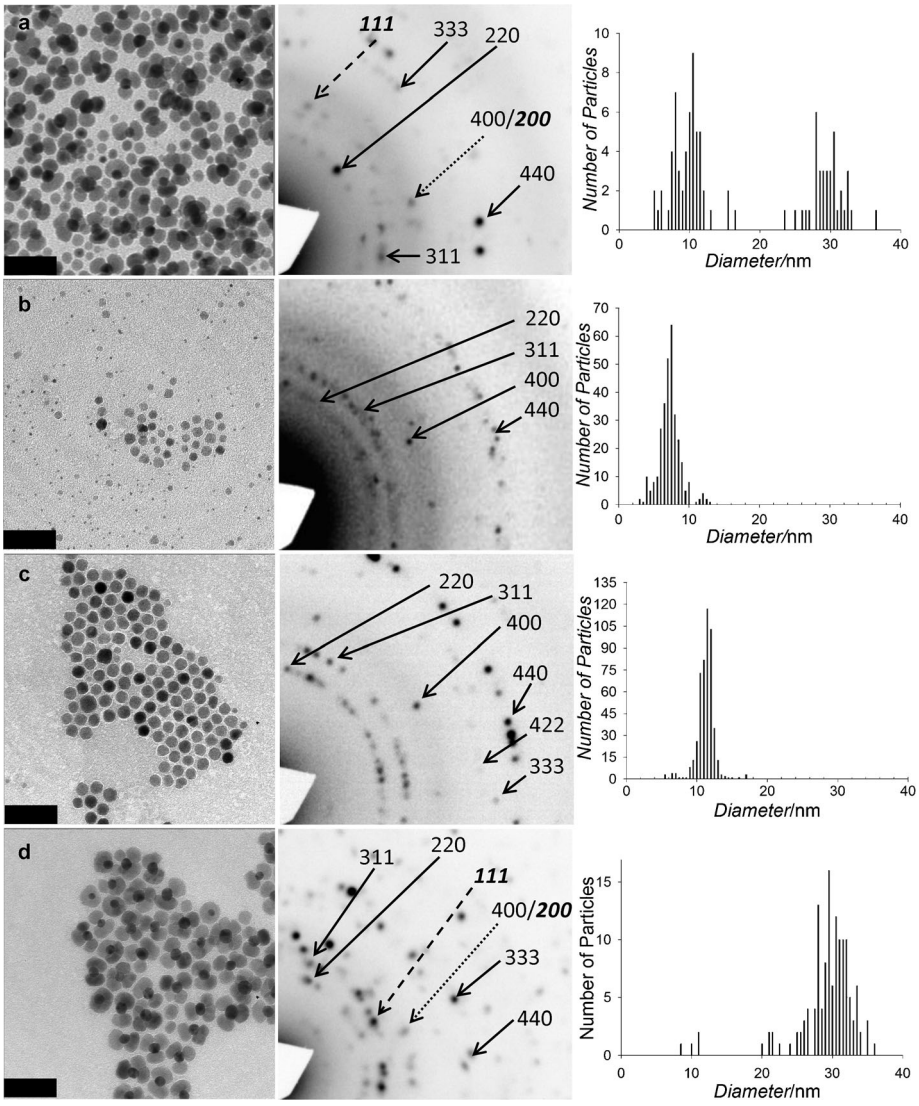

Figure 2. TEM images (scale bars are 50 nm), SAED patterns (labels with solid lines are Fe_3O_4; italics with dashed lines are Au), and size distribution histograms of a) the as-synthesized Au-Fe_3O_4 nanoparticles and the fractions from the DMCR peaks b) B, c) C, and d) D in Figure 1.

insights into the synthetic pathway. Based on earlier studies of spherical nanoparticles,[19a,b] nonmagnetic Au nanoparticles would be expected to elute in the first fraction (i.e., peak B), but evidence for individual Au nanoparticles without attached Fe_3O_4 is not observed. This suggests that Au nanoparticles nucleate the growth of Fe_3O_4, consistent with the accepted hybrid nanoparticle formation mechanism that involves heterogeneous nucleation of Fe_3O_4 on Au seeds. However, the presence of two distinct populations of individual Fe_3O_4 particles indicates that these also nucleate and grow under the same reaction conditions.

Retention of the Au-Fe_3O_4 heterostructures in the capillary at lower magnetic flux densities than the spherical Fe_3O_4 particles is indicative of their greater magnetic moments. Figure 3 compares the field cooled (FC) and zero field cooled

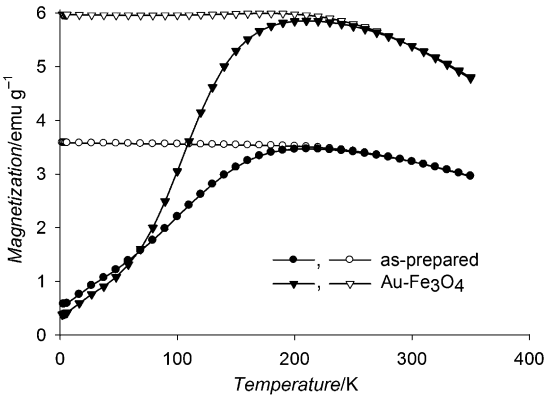

Figure 3. FC (open symbols) and ZFC (filled symbols) magnetization data. $H = 100$ Oe.

(ZFC) magnetization data for the purified Au-Fe_3O_4 heterostructures and the as-synthesized sample. The purified multimers exhibit a 20% higher saturation magnetization and a larger hysteresis than the as-synthesized sample at 5 K (Figure S6). The ZFC curves show that the purified sample has a 60% higher magnetization at T_B than the as-synthesized multimer sample. It is clear that impurities in the as-synthesized sample have a dramatic impact on the measured magnetic properties. Purification by DMCR separation yields the target Au-Fe_3O_4 heterostructures even when the synthetic method fails to generate a sample of desired particle uniformity.

FePt-Fe_3O_4 heterodimers were also analyzed using DMCR separation. The synthesis involved a one-pot, two-step reaction that has been reported to yield hybrid bimagnetic dimer nanoparticles.[9] A representative TEM image of the as-synthesized sample is shown in Figure 4a. Two populations of particles are observed, with average diameters of (2.7 ± 0.8) nm ($n = 88$) and (8.8 ± 0.9) nm ($n = 279$). The sample consists predominantly (75%) of heterodimers of FePt adhered to Fe_3O_4. A hexane solution of this sample was injected into the DMCR apparatus, and three peaks, B′, C′ and D′, were observed in the DMCR chromatogram (Figure 5) that eluted with 2, 0.5, and 0 T applied magnetic flux densities, respectively. TEM images of these fractions are

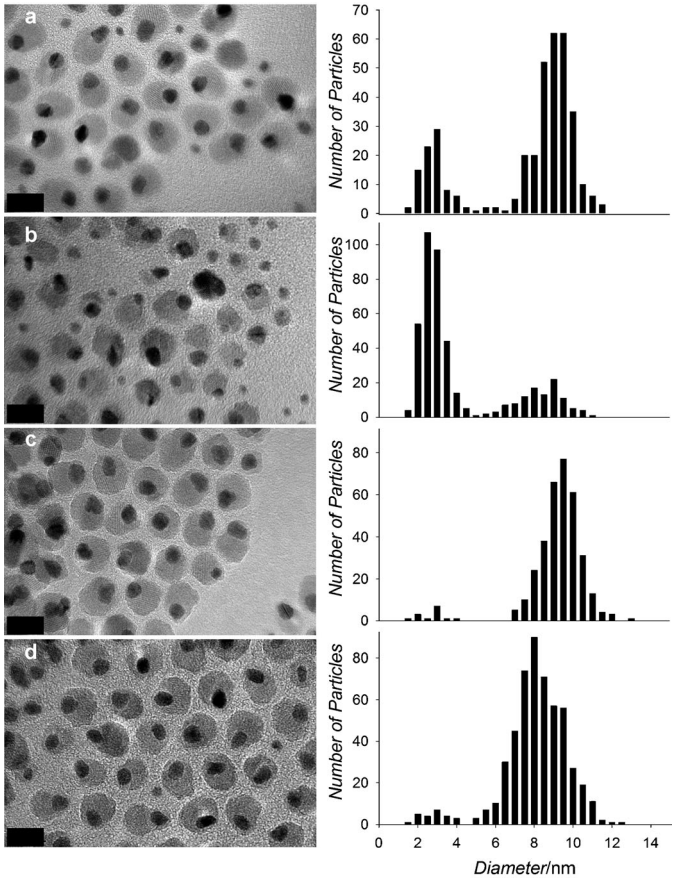

Figure 4. TEM images (scale bars are 10 nm) and size distribution histograms of a) the as-synthesized FePt-Fe_3O_4 particles and the fractions from the DMCR peaks b) B′, c) C′, and d) D′ in Figure 5.

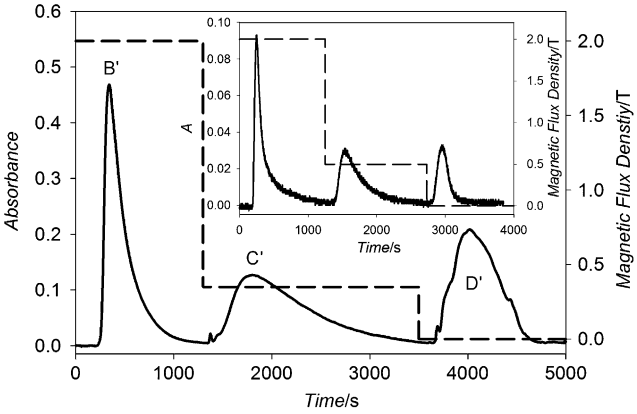

Figure 5. Chromatogram of preparatory-scale separation of FePt-Fe_3O_4 (solid line) and the magnetic field program used (dashed line). Inset is analytical-scale separation of the same sample. Hexane mobile phase is used for all separations.

shown in Figure 4b–d and Figure S7. Peak B′ contains small ((2.4 ± 0.5) nm, $n = 210$) particles, along with dimers having diameters of (8.1 ± 1.2) nm ($n = 105$) that comprise 33% of the sample. TEM images of peaks C′ and D′ show predominantly dimers with average diameters that are the same within experimental certainty ((9.1 ± 0.9) nm, $n = 333$, and

(8.1 ± 1.2) nm, $n = 502$, respectively), with only a few small-diameter particles ((2.5 ± 0.7), $n = 14$ and (2.8 ± 1.0) nm, $n = 26$, respectively). HRTEM images of the single particles (Figure S8) reveal lattice spacings that indicate these are predominantly Pt. Preparatory-scale DMCR was used to generate larger-scale samples, and powder X-ray diffraction (XRD) patterns for the separated fractions confirm that the as-synthesized particles and each of the separated fractions contain both Fe_3O_4 and FePt (Figure S9).

Because DMCR separates magnetic nanoparticles based on differences in their magnetic moments, the fractionation of the FePt-Fe_3O_4 sample into two populations (peaks C′ and D′) that have the same crystalline phases and statistically the same compositions and average diameters of Fe_3O_4 suggests that there is a polydispersity of magnetic moment within the FePt-Fe_3O_4 nanoparticle heterostructures. This was consistently observed in several separately prepared FePt-Fe_3O_4 samples. Figure 6 shows the FC and ZFC magnetization data for each isolated fraction. At 300 K (the temperature of the

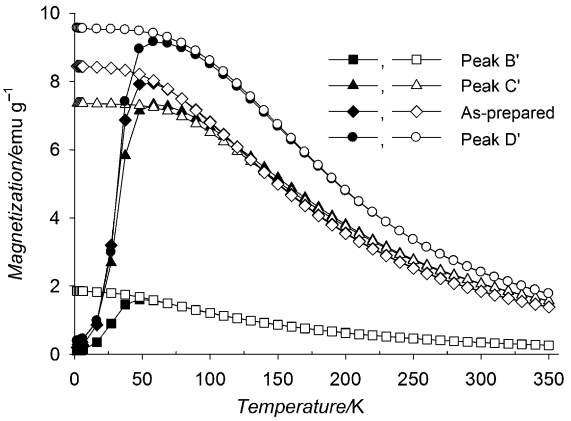

Figure 6. FC (open symbols) and ZFC (filled symbols) magnetization curves of the as-synthesized FePt-Fe_3O_4 particles compared to particles isolated from the indicated peaks in the chromatogram. $H = 100$ Oe.

DMCR separation), the magnetization of the particles that eluted in peak B′ is significantly lower than that of the particles eluted in peak C′. The purified dimers from peak D′ have a higher magnetization than the as-synthesized sample, highlighting the polydispersity in magnetic properties that result from a typical synthesis of FePt-Fe_3O_4 hybrid nanoparticles.

The dispersity in magnetic moments can be rationalized by a variation of the Fe:Pt ratio in the FePt component of the dimers, as suggested by EDS and ICP-AES data (Figure S10). Particles from fraction B′ contain more Pt than the as-synthesized sample because of the presence of small Pt nanoparticles, and the amount of Pt decreases for the second and third dimer fractions. ICP-AES indicates that the Fe content is higher for particles in fractions C′ and D′, mirroring the observed increase in magnetization. Together, the data suggest that although the nanoparticle dimers in the three fractions have essentially identical morphologies and sizes as observed by TEM, differences in their chemical composition give rise to polydispersity in magnetic moments.

In conclusion, DMCR was used to separate and purify hybrid magnetic nanoparticles, which are challenging to synthesize as pure samples in high yield because of the competition between heterogeneous seeded growth and the nucleation of isolated particles under the same reaction conditions. DMCR enables interrogation of the magnetic properties of pure samples that are free from ensemble averaging effects, which are otherwise unavoidable (and often undetectable using the most traditional and well-established characterization tools) in as-synthesized samples.

Experimental Section

Synthesis: Full experimental details are included in the Supporting Information and are based on literature procedures for Au and Au-Fe_3O_4,[3] and FePt-Fe_3O_4 nanoparticles.[9] Briefly, Au nanoparticles were synthesized from H[$AuCl_4$] in oleylamine at 85–90 °C. Au-Fe_3O_4 was prepared by injecting [$Fe(CO)_5$] into a mixture of oleic acid and octadecene at 120 °C, followed by addition of Au nanoparticles in hexanes and refluxing for 30 min. FePt-Fe_3O_4 dimers were made by reacting [$Pt(acac)_2$] in octadecene with [$Fe(CO)_5$] and oleic acid at elevated temperature. All nanoparticles were isolated by repeated precipitation with ethanol or 2-propanol followed by centrifugation and redispersion in hexanes.

Purification: DMCR purification was performed using a previously described apparatus.[19a,b] Analytical- and preparatory-scale DMCR separations were performed using 250 and 700 μm diameter capillaries, respectively, with a hexane mobile phase and an applied magnetic flux density of up to 2 T.

Characterization: Low-resolution TEM images were acquired using a JEOL-1200EXII TEM operating at 80 keV. HRTEM images, EDS, and SAED patterns were collected using JEOL-2010 LaB_6 and JEOL-2010F. UV/vis absorbance spectra were obtained with a Cary 500 spectrometer. XRD data were collected on a Bruker Advance D8 X-ray diffractometer using $Cu_{K\alpha}$ radiation. DC magnetization measurements were performed using a Quantum Design SQUID magnetometer. Experimental details are described in the Supporting Information.

Received: July 11, 2011
Published online: September 6, 2011

Keywords: heterostructures · hybrid nanocrystals · magnetic nanoparticles · nanostructures · purification

[1] a) R. Costi, A. E. Saunders, U. Banin, *Angew. Chem.* **2010**, *122*, 4996; *Angew. Chem. Int. Ed.* **2010**, *49*, 4878; b) C. Wang, C. Xu, H. Zeng, S. Sun, *Adv. Mater.* **2009**, *21*, 3045; c) P. D. Cozzoli, T. Pellegrino, L. Manna, *Chem. Soc. Rev.* **2006**, *35*, 1195.
[2] a) C. Wang, H. Yin, S. Dai, S. Sun, *Chem. Mater.* **2010**, *22*, 3277; b) Y. Lee, M. A. Garcia, N. A. Frey Huls, S. Sun, *Angew. Chem.* **2010**, *122*, 1293; *Angew. Chem. Int. Ed.* **2010**, *49*, 1271.
[3] H. Yu, M. Chen, P. M. Rice, S. X. Wang, R. L. White, S. Sun, *Nano Lett.* **2005**, *5*, 379.
[4] H. Gu, Z. Yang, J. Gao, C. K. Chang, B. Xu, *J. Am. Chem. Soc.* **2005**, *127*, 34.
[5] C. Xu, B. Wang, S. Sun, *J. Am. Chem. Soc.* **2009**, *131*, 4216.
[6] C. Xu, J. Xie, D. Ho, C. Wang, N. Kohler, E. G. Walsh, J. R. Morgan, Y. E. Chin, S. Sun, *Angew. Chem.* **2008**, *120*, 179; *Angew. Chem. Int. Ed.* **2008**, *47*, 173.
[7] C. Wang, H. Daimon, S. Sun, *Nano Lett.* **2009**, *9*, 1493.
[8] H. Yin, C. Wang, H. Zhu, S. H. Overbury, S. Sun, S. Dai, *Chem. Commun.* **2008**, 4357.

[9] A. Figuerola, A. Fiore, R. D. Corato, A. Falqui, C. Giannini, E. Micotti, A. Lascialfari, M. Corti, R. Cingolane, T. Pellegrino, P. D. Cozzoli, L. Manna, *J. Am. Chem. Soc.* **2008**, *130*, 1477.
[10] Y. Li, Q. Zhang, A. V. Nurmikko, S. Sun, *Nano Lett.* **2005**, *5*, 1689.
[11] T. Mokari, E. Rothenberg, I. Popov, R. Costi, U. Banin, *Science* **2004**, *304*, 1787.
[12] R. Costi, A. E. Saunders, E. Elmalem, A. Salant, U. Banin, *Nano Lett.* **2008**, *8*, 637.
[13] M. Casavola, R. Buonsanti, G. Caputo, P. D. Cozzoli, *Eur. J. Inorg. Chem.* **2008**, 837.
[14] W. Shi, H. Zeng, Y. Sahoo, T. Y. Ohulchanskyy, Y. Ding, Z. L. Wang, M. Swihart, P. N. Prasad, *Nano Lett.* **2006**, *6*, 875.
[15] L. Carbone, P. D. Cozzoli, *Nano Today* **2010**, *5*, 449.
[16] Y. Wei, R. Klajn, A. O. Pinchuk, B. A. Grzybowski, *Small* **2008**, *4*, 1635.
[17] a) G. Chen, Y. Wang, L. H. Tan, M. Yang, L. S. Tan, Y. Chen, H. Chen, *J. Am. Chem. Soc.* **2009**, *131*, 4218; b) R. P. Carney, J. Y. Kim, H. Qian, R. Jin, H. Mehenni, F. Stellacci, O. M. Bakr, *Nat. Commun.* **2011**, *2*, 335; c) J. Gigault, B. K. Gale, I. Le Hécho, G. Lespes, *Anal. Chem.* **2011**, DOI: 10.1021/ac2008948.
[18] B. Kowalczyk, I. Lagzi, B. A. Grzybowski, *Curr. Opin. Colloid Interface Sci.* **2011**, *16*, 135.
[19] a) J. S. Beveridge, J. R. Stephens, A. H. Latham, M. E. Williams, *Anal. Chem.* **2009**, *81*, 9618; b) J. S. Beveridge, J. R. Stephens, M. E. Williams, *Analyst* **2011**, *136*, 2564; c) A. H. Latham, R. Freitas, P. Schiffer, M. E. Williams, *Anal. Chem.* **2005**, *77*, 5055.
[20] J. Xie, M. Aronova, L. Zhu, X. Lin, Q. Quan, G. Liu, G. Zhang, K. Choi, K. Kim, X. Sun, S. Lee, S. Sun, R. Leapman, X. Chen, *ACS Nano* **2011**, *5*, 3043.

